Numerical Investigation of Hydroelastic Response of a Three-Dimensional Deformable Hydrofoil

Saeed HOSSEINZADEH[a,1] and Kristjan TABRI[a]

[a] *Tallinn University of Technology, Ehitajate tee 5, 19086 Tallinn, Estonia*

Abstract. The present study is concerned with the numerical simulation of Fluid-Structure Interaction (FSI) on a deformable three-dimensional hydrofoil in a turbulent flow. The aim of this work is to develop a strongly coupled two-way fluid-structure interaction methodology with a sufficiently high spatial accuracy to examine the effect of turbulent and cavitating flow on the hydroelastic response of a flexible hydrofoil. A 3-D cantilevered hydrofoil with two degrees-of-freedom is considered to simulate the plunging and pitching motion at the foil tip due to bending and twisting deformation. The defined problem is numerically investigated by coupled Finite Volume Method (FVM) and Finite Element Method (FEM) under a two-way coupling method. In order to find a better understanding of the dynamic FSI response and stability of flexible lifting bodies, the fluid flow is modeled in the different turbulence models and cavitation conditions. The flow-induced deformation and elastic response of both rigid and flexible hydrofoils at various angles of attack are studied. The effect of three-dimension body, pressure coefficient at different locations of the hydrofoil, leading-edge and trailing-edge deformation are presented and the results show that because of elastic deformation, the angle of attack increases and it lead to higher lift and drag coefficients. In addition, the deformations are generally limited by stall condition and because of unsteady vortex shedding, the post-stall condition should be considered in FSI simulation of deformable hydrofoil. To evaluate the accuracy of the numerical model, the present results are compared and validated against published experimental data and showed good agreement.

Keywords. Fluid-Structure Interaction; Flow-induced vibration; Deformable Hydrofoil; Turbulence Models; Cavitation

1. Introduction

The interaction between fluid and structure (FSI) plays a vital role in aero-hydro dynamics applications particularly in marine propellers and lifting bodies such as hydrofoils, turbine blades, and wings. In recent decades, there has been increased interest to use composite materials for marine structures such as propellers, rudders, hydrofoil supported catamarans, etc. Using flexible structures may be subject to uncontrolled static and dynamic instabilities that can lead to vibration, resonance, and performance breakdown. In the case of hydrofoil supported catamaran (HYSUCAT) and sailing boats equipped with hydrofoil and wing-sails, it is important to investigate the performance of these boats during high speed and near-surface operations [1]. During the high-speed operations, the hydrofoils may face cavitation condition that is indeed a serious concern for the hydrofoil performance [2]. Furthermore, the existence of cavity can lead to

[1] Corresponding Author, Saeed Hosseinzadeh, Tallinn University of Technology, Ehitajate tee 5, 19086 Tallinn, Estonia; E-mail: saeed.hosseinzadeh@taltech.ee

hydroelastic stability problems such as flow-induced vibrations, resonance, buffeting, and flutter for lightweight hydrofoils [3].

Previous research has established some numerical [4–14] and experimental [15–19] studies for examining the hydroelastic effects on lift and drag coefficients of deformable lifting bodies. To provide the FSI simulation, there are two approaches for coupling the fluid and solid domains. The one- way coupling and two-way coupling reflect how the hydrodynamic loads and displacements are transferred between the fluid and structure domains. Ducoin et al. [5] used a one-way numerical method to examine a deformable hydrofoil with transient pitching motion at moderate Reynolds number. Although there was good agreement with the experiments at low pitching velocities but for the highest pitching velocities, there was still some numerical discrepancy. Benra et al. [8] evaluated the one-way and two-way coupling methods for numerical simulation of fluid-structure interactions on a simple case and presented that the results of two-way coupling method were more accurate, particularly for larger deflections where structural deformation significantly affects the fluid field. Furthermore, a comparison between one-way and two-way coupling method for flexible hydrofoils conducted by Huang et al. [6]. To date, several studies have investigated the hydroelastic response of a two-dimensional flexible hydrofoil. Ducoin and Young [10] provided a numerical approach based on a simple 2-DOF system and simulated the bending and twisting deformations of a 2D hydrofoil. They used the Loose Hybrid Coupled (LHC) coupling method for FSI solvers which presented by Chae et al., [20] and Young et al., [21]. In 2014, Akcabay et al. [3] simulated the cavity-induced vibrations on 2D flexible hydrofoils and investigated the influence of foil vibrations on the cavity and vorticity dynamics, and resultant load variations. Due to ignoring three-dimensional effects, some errors observed for the magnitudes of the induced deformations, but in general, there was a reasonable agreement between numerical predictions and experimental measurements. Chae et al. [11] studied the influence of the flow-induced bend–twist coupling of flexible hydrofoils and comparing the inviscid and viscous fluid-structure interaction simulation of cantilevered NACA0015 hydrofoils in water. The 3D effects were neglected in their FSI method. They used 2D URANS for the simulation, which was not sufficient and noted that high fidelity, 3D simulation with a very fine mesh, and very small time step size are needed. The numerical stability behavior of the LHC method examined by Akcabay et al. [12]. In 2018, Wu et al. [13] used a hybrid coupled fluid-structure interaction model and applied 3D effects on [3] and [20] FSI method. They investigated the transient characteristics of cavitating flow over a flexible 2D hydrofoil via combined experimental and numerical studies and concluded that the transient cavitating behaviors lead to the periodic pressure fluctuation on the hydrofoil. Mortazavinia et al, [14] analyzed a three-dimensional flexible hydrofoil in viscous flow by using a two-way strong coupling method and observed reasonable agreement between numerical results and experimental data and concluded that the small differences between the experimental and numerical results are due to the influence of tip gap flow, which was ignored in their study.

The objectives of this study are to investigate the effect of turbulent and cavitating flow on the hydroelastic response of a flexible hydrofoil; and examine the three-dimensional effects both for rigid and flexible hydrofoils to gain greater insight into the elastic effect on highly flexible hydrofoils. The next section of this paper will describe the numerical FSI setup and examine different turbulence models to find accurate results compared to the experimental data. After validating the numerical model, the effect of three-dimension body, pressure coefficient at different locations of the hydrofoil, leading-edge, and trailing-edge deformation will present in the result section.

2. Numerical Modeling

In this study, the fluid-structure interaction problem of a three-dimensional flexible hydrofoil is numerically studied with the Finite Volume Method (FVM) and Finite Element Method (FEM) under a two-way coupling method using the commercial Star CCM+ software. The governing equations for both fluid and structural domains are presented in the next subsection.

2.1. Governing equations and domains description

The flow around the hydrofoil is assumed as incompressible and viscous fluids and modeled by the Unsteady Reynolds Averaged Navier–Stokes (URANS) equations. The mass continuity and the Navier-Stokes equations can be written on differential form as

$$\frac{\partial \rho}{\partial t} + \nabla.(\rho \mathbf{v}) = 0 \tag{1}$$

$$\rho(\frac{\partial \mathbf{v}}{\partial t} + \mathbf{v}.\nabla \mathbf{v}) = -\nabla p + \nabla.[(\mu + \mu_t^*)(\nabla \mathbf{v} + \nabla \mathbf{v}^T)] \tag{2}$$

Where **v** is the local velocity of the fluid, ρ is the fluid density, μ is the fluid viscosity, p is the pressure and μ_t^* is the turbulence eddy viscosity for the URANS model. It should be noted that for the cavity flow the mixture density and viscosity is considered. The presence of cavitation is determined by computing the vapor volume fraction, α_v , through formulating a transport equation for α_v, and solving it using the Volume of Fluid (VOF) method. As shown, the density ρ_f and the dynamic viscosity μ_f of the fluid mixture are represented as functions of the vapor density and viscosity, liquid density and viscosity, and volume fraction of vapor α_v:

$$\rho_f = \alpha_v.\rho_v + (1-\alpha_v).\rho_w \tag{3}$$

$$\mu_f = \alpha_v.\mu_v + (1-\alpha_v).\mu_w \tag{4}$$

Where *w* and *v* subscripts are for water and vapor, respectively. In addition, for modeling the cavity flow Schnerr-Sauer cavitation model [22] is used. The relationship between the vapor volume fraction α_v and the vapor bubble radius R is given by:

$$\alpha_v = n_0.\frac{4}{3}\pi R^3 \Big/ (1 + n_0.\frac{4}{3}\pi R^3) \tag{5}$$

Where n_0 is the bubble density per cubic meter. The volume fraction of the vapor is α_v and the governing equation on α is:

$$\frac{\partial \alpha_v}{\partial t} + \nabla.(\alpha_v \mathbf{v}) = (\frac{n_0}{1 + n_0.\frac{4}{3}\pi R^3})\frac{d}{dt}(\frac{4}{3}\pi R^3) \tag{6}$$

The structural part of the problem is solved using the finite element method. A three-dimensional cantilevered flexible hydrofoil with two degrees-of-freedom is considered to simulate the plunging and pitching motion at the foil tip due to bending and twisting deformation. The displacements are described by δ to numerically solve the problem, and the dynamic equation of motion with respect to a fixed solid body can be written as follows

$$M\ddot{\delta} + K\dot{\delta} + C\delta = F(t) \tag{7}$$

Where M, K, and C are the structural mass, stiffness, and damping n×n matrix, respectively. The linear elasticity is considered for structural solver. As reported by Benra et al. [8] and Huang et al. [6] the results of the two-way coupling method are more accurate and closer to the experimental data, particularly for larger deflections. Therefore, the two-way coupling method is applied to the numerical simulation in this study.

The schematic of the problem considered in this study is illustrated in Figure 1. As shown in this figure, the numerical fluid domain is 15c length, 1.28c wide and 1.28c tall. The foil leading edge is at 4.5c from the inlet, and the foil trailing edge is at 9.5c from the outlet. The reason for using the confined fluid domain instead of the infinite fluid domain is that the numerical results obtained using the confined mesh matched better with the experimental measurements [7]. The foil is clamped to the back wall (root section) and is free on the tip section. In order to find accurate results, compared with the experiment, 1 mm gap between the free tip of the hydrofoil and the other end of the domain wall is considered in the defined numerical setup. As shown in Figure 1, for all the cases presented in this study, the NACA66 hydrofoil with a chord length c =0.15 m, and span length b=0.191 m is considered. At the inlet boundary, a constant turbulent intensity of 2.95% is applied, which is equal to the experimentally measured turbulent intensity [3].

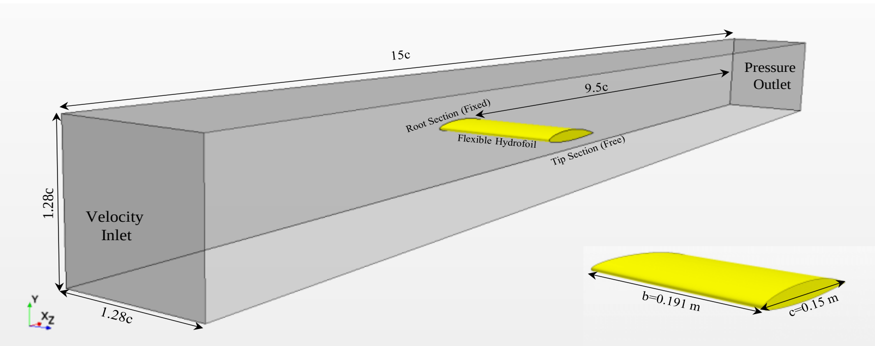

Figure 1. The schematic of the three-dimensional numerical setup

2.2. Mesh setup

The generated mesh for both fluid and structure domain are shown in Figure 2. The finite volume method (FVM) is used for the fluid solver and the governing equations are discretized over a grid of cells, with nodal values of the physics fields at the center of each cell. For the fluid domain, a grid is built up by polyhedral cells that lead to an accurate solution and is particularly well suited for this study. The fluid domain is discretized with 5694289 cells and the smallest elements are taken near the hydrofoil walls. The Minimum grid size is 0.005 m at the fluid region and a refinement with 0.001 m grid size is considered around the hydrofoil. As the mesh has to be updated to account for the deformations, the mesh morpher model is employed. Furthermore, For the structural domain, the finite element method with quadrilateral mesh is applied. The structural region is discretized with 112500 cells and 5e-5 m minimum grid size. The time-step size for both the fluid and solid solvers is selected to be $\Delta t=5\times10^{-4}$ s with 15 internal iterations. During the simulation, care was taken to ensure that the mesh and time-step size are fine enough to limit mesh distortion issues after each structural calculation.

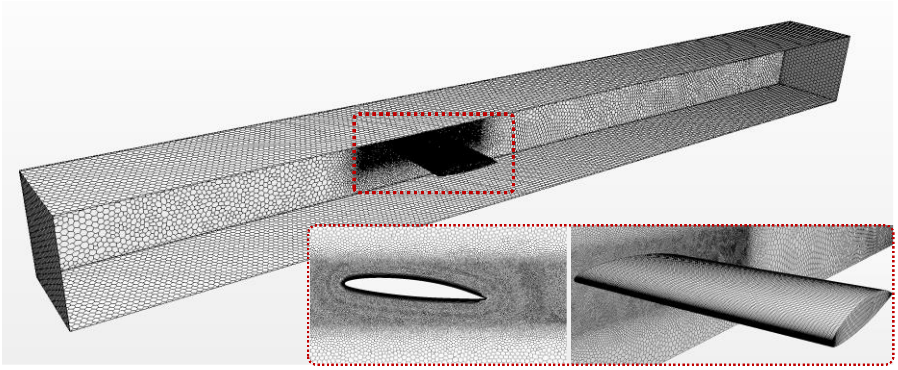

Figure 2. Generated mesh on the fluid and structure domain and a close-up view near the foil

2.3. Validation

To verify the hydroelastic response of the flexible hydrofoil, the experiments presented by [15] and [18] are chosen for comparison. In the first part of the validation, the hydrofoil simulated in Re=750000 and α_0=8º as the initial angle of attack of the foil. The density and dynamic viscosity of fluid are taken to be ρ_l=997.56 kg/m^3 and μ_l=8.887×10^{-4} kg/(ms), respectively. The twisting angle of the hydrofoil can be calculated from the difference between the vertical deformation of the leading edge ($\delta_{yleading}$) and trailing edge ($\delta_{ytrailing}$). To examine the hydroelastic effect on the hydrofoil performance, the results of rigid and flexible hydrofoil are compared in this section. The rigid hydrofoil is made of stainless-steel with Young's modulus, density, and Poisson's ratio E_s=210 GPa, ρ_s =7800 kg/m^3, and ν_s=0.3, respectively. Moreover, the flexible hydrofoil is made of a POM polyacetate with E_s=3 GPa, ρ_s=1480 kg/m^3, and ν_s=0.35.

As shown in Figure 3, the results of the rigid hydrofoil are first compared against the experiment [15] at two different initial angle of attack, and very good agreement is observed.

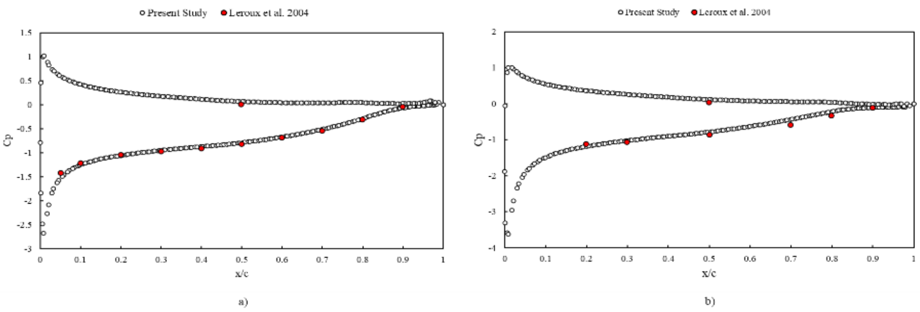

Figure 3. Comparison of the computed pressure coefficient against experimental data [15] for the rigid hydrofoil a) α=6º b) α=8º

Figure 4a) shows a comparison between the computed lift and drag coefficients and experiment [10] at different angles of attack for the rigid hydrofoil. The maximum tip section deformations of the flexible hydrofoil are shown in Figure 4b). Good agreements are observed for both lift coefficient and tip displacement that means the present numerical model can predict the hydroelastic effect well. In addition, it shows that the deformation of the flexible hydrofoil highly influences the flow around the body. As shown in Figure 4b), the deformation is within 2.4 mm under 5°, but gradually increases to 4.5 mm at 12°. At higher attack angles (α>8°), the higher discrepancy is observed.

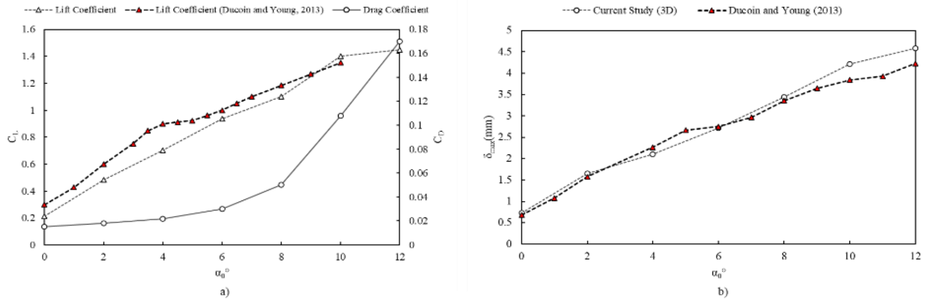

Figure 4. Comparison of the computed results against experimental data [10] at different initial angle of attack a) the lift and drag coefficients of the rigid hydrofoil b) the maximum tip section deformations of the flexible hydrofoil

In order to gain better insight into the effect of the turbulence models on hydroelastic problems, different turbulence models are applied to the numerical setup. It should be noted that the non-cavity flow is considered for these simulations. As shown in Table 1, although the results of the K-Omega Detached Eddy Simulation (DES) turbulence model are closer to the experiment, the numerical instability in this model increases. In addition, as noted in Ducoin et al. [23], the standard turbulence models tend to overestimate the turbulent eddy viscosity in the cavity region, therefore, the k–ω Shear Stress Transport (SST) turbulence model is used for the simulations.

Table 1. Comparison of the lift and drag coefficients, bending and twisting deformations for the flexible hydrofoil at Re=750000, α_0=8°, and non-cavitating flows

	K-Omega SST	**K-Epsilon Two layer**	**DES (K-Omega Detached Eddy)**	**2D K-Omega SST (Akcabay et al., 2014) [3]**	**Experiment (Ducoin et al., 2012a) [18]**
C_D	0.047	0.0547	0.0487	0.022	-
C_L	0.98	1.01	0.88	1.22	-
δ_y/c	0.02293	0.02286	0.023	0.01	0.024
Δα (deg)	-0.305	-0.258	-0.285	-0.18	-0.39

Furthermore, the computed numerical results are compared with the experimental data for the rigid and flexible hydrofoils at α_0=8° both for cavity and non-cavity flows and good agreement is observed particularly for cavity flows. As shown in Table 2, compared with previous two-dimensional numerical simulation [3], the results of the current study are matched better with the experiments. Therefore, the three-dimension effect is significant on the flexible hydrofoil and needs to be considered for the simulation of flexible lifting bodies.

Table 2. Comparison of the lift and drag coefficients, bending and twisting deformations for the rigid and flexible hydrofoils at α_0=8°

		C_D	C_L	δ_y/c	**Δα (deg)**
Rigid	Experiment (Leroux et al. 2004)	0.048	1.065	-	-
	Computation 2D (Akcabay et al., 2014)	0.022	1.19	-	-
	Present study 3D	0.0416	1.02	-	-
Flexible	Experiment (Ducoin et al., 2012a)	-	-	0.024	-0.39
	Computation 2D (Akcabay et al., 2014)	0.022	1.22	0.01	-0.18
	Present 3D study (No cavity flow)	0.047	0.98	0.0229	-0.305
	Present 3D study (cavity flow)	0.05	1.1	0.0247	-0.35

3. Results

The results of the current paper are presented in this section. The effect of cavitation on the deformations, pressure distribution at different cavitation numbers (σ), and bending deformation at the various angles of attack are studied. As shown in Figure 1, the deformed and undeformed tip section of the flexible hydrofoil are compared with experimental values for non-cavity and cavity flows. The numerical maximum tip deformation and twist angle for the non-cavity flow are δ_y= 3.435 mm and θ= −0.305°, respectively, compared with the experiment value of δ_y= 3.4 mm and θ= −0.4°. For the cavitation number σ=2.6, the bending and twisting deformations are δ_y= 3.705 mm and θ= −0.35, respectively, in comparison with the experiment values of δ_y= 3.6 mm and θ= −0.39°.

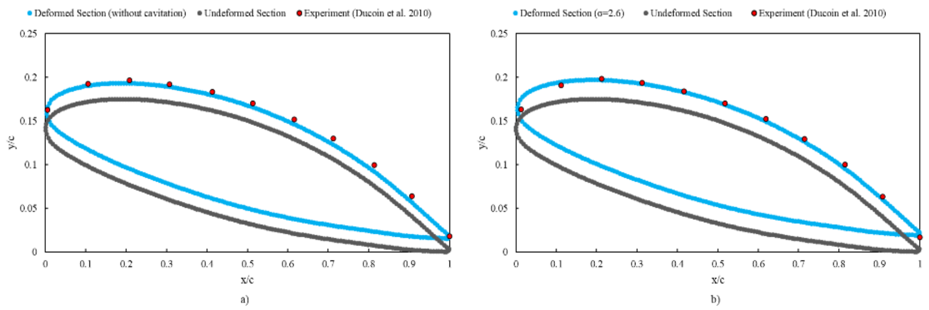

Figure 5. Comparison of the present numerical and experimental deformed tip section a) without cavitation b) cavity flow with cavitation number σ=2.6

The effect of cavity flow on pressure distribution along the hydrofoil surface at three different sections for two cavitation numbers are depicted in Figure 6. The three-dimensional effects are shown in this figure by considering z/b=0, as the fixed root section of the hydrofoil, and z/b=1 as the hydrofoil free tip section.

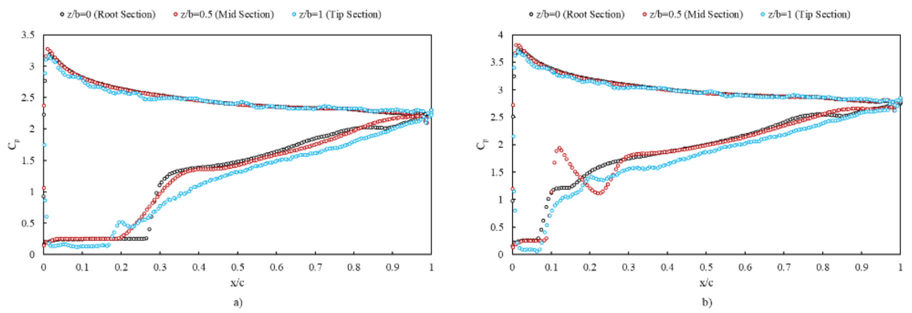

Figure 6. Comparison of the pressure coefficient along the hydrofoil surface at three different sections at Re=750000 and α_0=8° a) σ=2 b) σ=2.6

The simulated cavitation patterns at three different cavitation numbers by volume fraction of vapor for the flexible hydrofoil are presented in Figure 7a). In addition, the effect of cavitation on the velocity at the free tip section of flexible hydrofoil is demonstrated in Figure 7b).

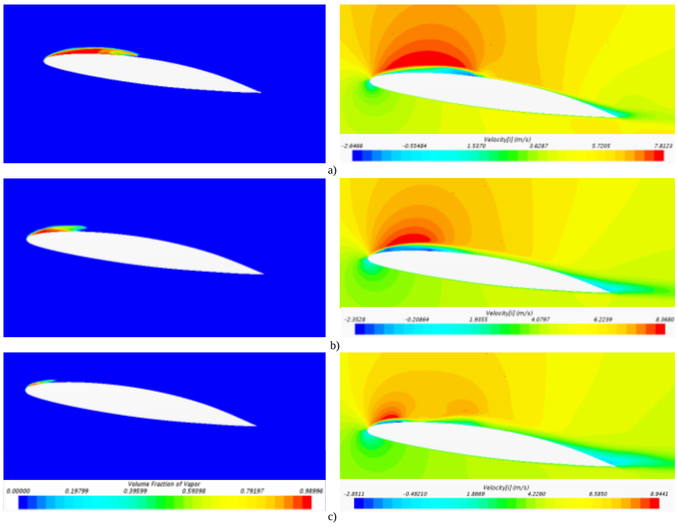

Figure 7. Simulated cavitation patterns presented by volume fraction of vapor for the flexible hydrofoil (left) and Velocity contours at the free tip section (right) at Re=750000 and α_0=8° a) σ=1.4 b) σ=2 c) σ=2.6

Furthermore, the hydroelastic response of three-dimensional flexible hydrofoil is investigated. The flow-induced deformation of both rigid and flexible hydrofoils at α=8° and Re=750000 are depicted in Figure 8. As expected, the deformation of the hydrofoil near the leading edge is greater than the value near the trailing edge. The effect of the angle of attack on the bending deformations is shown in Figure 9.

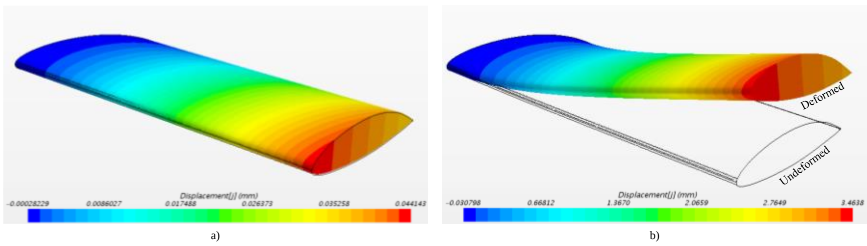

Figure 8. Vertical mesh displacement contour at Re=750000 and α_0=8° of 3D foil a) the rigid hydrofoil b) the flexible hydrofoil

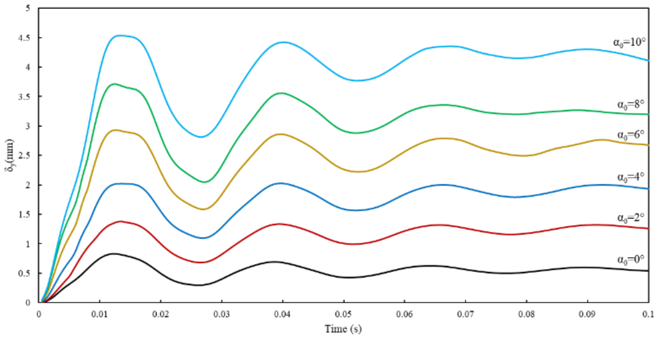

Figure 9. Time histories of vertical bending deformation at different initial angles of attack

4. Conclusions

The main aim of this paper has been to investigate the hydroelastic response of a three-dimensional flexible hydrofoil by establishing a numerical model to conducted coupled simulations between a fluid and structure domain. This has been achieved by using commercial STAR CCM+ software. The problem is simulated by coupling FVM and FEM through using a strong two-way coupling approach. The validity of the proposed model evaluated by comparing the results of the current study against previously published experimental data and good agreement between the numerical results and experimental data observed. To find a better understanding of the dynamic FSI response and stability of flexible hydrofoil, the fluid flow modeled in the different turbulence models and cavitation conditions. The flow-induced deformation and elastic response of both rigid and flexible hydrofoils at various angles of attack studied. The effect of three-dimension body, pressure coefficient at different locations of the hydrofoil, leading-edge and trailing-edge deformation presented. The results show that because of elastic deformation, the angle of attack increases, and it leads to higher lift and drag coefficients. In addition, because of better agreement between the results of current 3D simulations and previous experimental data, the three-dimensional effect on the flexible hydrofoil is considerable.

References

[1] M. Sacher *et al.*, "Flexible hydrofoil optimization for the 35th America's Cup with constrained EGO method," *Ocean Eng.*, vol. 157, pp. 62–72, Jun. 2018.

[2] M. Sedlar, B. Ji, T. Kratky, T. Rebok, and R. Huzlik, "Numerical and experimental investigation of three-dimensional cavitating flow around the straight NACA2412 hydrofoil," *Ocean Eng.*, vol. 123, pp. 357–382, Sep. 2016.

[3] D. T. Akcabay, E. J. Chae, Y. L. Young, A. Ducoin, and J. A. Astolfi, "Cavity induced vibration of flexible hydrofoils," *J. Fluids Struct.*, vol. 49, pp. 463–484, Aug. 2014.

[4] A. Ducoin, F. Deniset, T. Damay, J.-A. Astolfi, and C. Laine, "Numerical Investigation of Deformable Hydrofoils in Steady Flows," in *Volume 4: Fluid Structure Interaction, Parts A and B*, 2006, vol. 2006, pp. 157–164.

[5] A. Ducoin, J. A. Astolfi, F. Deniset, and J. F. Sigrist, "Computational and experimental investigation of flow over a transient pitching hydrofoil," *Eur. J. Mech. B/Fluids*, vol. 28, no. 6, pp. 728–743, Nov. 2009.

[6] Z. Huang, Y. Xiong, and Y. Xu, "The simulation of deformation and vibration characteristics of a flexible hydrofoil based on static and transient FSI," *Ocean Eng.*, vol. 182, pp. 61–74, Jun. 2019.

[7] A. Ducoin and Y. L. Young, "Hydroelastic Response and Stability of a Hydrofoil in Viscous Flow," 2011.

[8] F.-K. Benra, H. J. Dohmen, J. Pei, S. Schuster, and B. Wan, "A Comparison of One-Way and Two-Way Coupling Methods for Numerical Analysis of Fluid-Structure Interactions," *J. Appl. Math.*, vol. 2011, p. 16, 2011.

[9] D. Tolga Akcabay and Y. Lu Young, "Cite as," *J. Appl. Phys.*, vol. 24, p. 26104, 2012.

[10] A. Ducoin and Y. L. Young, "Hydroelastic response and stability of a hydrofoil in viscous flow," *J. Fluids Struct.*, vol. 38, pp. 40–57, Apr. 2013.

[11] E. J. Chae, D. T. Akcabay, and Y. L. Young, "Influence of flow-induced bend–twist coupling on the natural vibration responses of flexible hydrofoils," *J. Fluids Struct.*, vol. 69, pp. 323–340, Feb. 2017.

[12] D. T. Akcabay, J. Xiao, and Y. L. Young, "Numerical stabilities of loosely coupled methods for robust modeling of lightweight and flexible structures in incompressible and viscous flows," *Acta Mech. Sin.*, vol. 33, no. 4, pp. 709–724, 2017.

[13] Q. Wu, B. Huang, G. Wang, and S. Cao, "The transient characteristics of cloud cavitating flow over a flexible hydrofoil," *Int. J. Multiph. Flow*, vol. 99, pp. 162–173, Feb. 2018.

[14] Z. Mortazavinia, R. Camarero, and F. Guibault, "Three-dimensional Analysis of Two-way Fluid-structure Interaction on a Flexible Hydrofoil in Viscous Flow," *Int. J. Fluid Mach. Syst.*, vol. 11, no. 3.

[15] J.-B. Leroux, J. A. Astolfi, and J. Y. Billard, "An Experimental Study of Unsteady Partial Cavitation," 2004.

[16] C. Münch, P. Ausoni, O. Braun, M. Farhat, and F. Avellan, "Fluid-structure coupling for an oscillating hydrofoil," *J. Fluids Struct.*, vol. 26, no. 6, pp. 1018–1033, Aug. 2010.

[17] R. E. A. Arndt, "Some remarks on hydrofoil cavitation," *J. Hydrodyn.*, vol. 24, no. 3, pp. 305–314, Jul. 2012.

[18] A. Ducoin, J. André Astolfi, and J. F. Sigrist, "An experimental analysis of fluid structure interaction on a flexible hydrofoil in various flow regimes including cavitating flow," *Eur. J. Mech. B/Fluids*, vol. 36, pp. 63–74, Nov. 2012.

[19] M. Sedlá, M. Komárek, M. Vyroubal, and M. Müller, "Experimental And Numerical Analysis of Cavitating Flow Around a Hydrofoil."

[20] E. Jung Chae, D. Tolga Akcabay, and Y. Lu Young, "Dynamic response and stability of a flapping foil in a dense and viscous fluid," *Phys. Fluids*, vol. 25, p. 104106, 2013.

[21] Y. Lu Young, E. Jung Chae, D. Tolga Akcabay, Y. L. Young, E. J. Chae, and D. T. Akcabay, "Hybrid algorithm for modeling of fluid-structure interaction in incompressible, viscous flows," *Acta Mech. Sin.*, vol. 28, no. 4, pp. 1030–1041, 2012.

[22] G. H. Schnerr and J. Sauer, "Physical and numerical modeling of unsteady cavitation dynamics," 2001.

[23] A. Ducoin, B. Huang, and Y. L. Young, "Numerical Modeling of Unsteady Cavitating Flows around a Stationary Hydrofoil," *Int. J. Rotating Mach.*, vol. 2012, p. 17, 2012.